EUROPEAN ORGANIZATION FOR NUCLEAR RESEARCH

CERN-EP/79-120
10 October 1979

THREE-DIMENSIONAL IMAGE RECONSTRUCTION FOR A POSITRON CAMERA WITH LIMITED ANGULAR ACCEPTANCE

D. Townsend,

Dept. of Nuclear Medicine,
Cantonal Hospital of Geneva, Geneva, Switzerland.

B. Schorr and A. Jeavons,

CERN, Geneva, Switzerland.

To be presented at the
IEEE Nuclear Science Symposium,
San Francisco, California,
October 17-19, 1979

THREE-DIMENSIONAL IMAGE RECONSTRUCTION FOR A POSITRON CAMERA WITH LIMITED ANGULAR ACCEPTANCE

D. Townsend,

Dept. of Nuclear Medicine,
Cantonal Hospital of Geneva, Geneva, Switzerland

B. Schorr and A. Jeavons,

CERN, Geneva, Switzerland

1. Introduction

In recent years much effort has been devoted to the problems of image reconstruction applied to the field of Computed Tomography (CT). In particular, following the original work of Radon[1], techniques for two-dimensional reconstruction have been extensively developed, one of the main objectives being the efficient implementation of the algorithms on a digital computer. The many practical applications of these developments are evidenced by the availability of a wide variety of transmission and emission CT scanners.

Although the distributions that are imaged are inherently three-dimensional, for technical and mathematical simplicity they are treated as a sequence of two-dimensional sections that may be stacked together to form the original three-dimensional distribution. This approach is reasonable for passive imaging with an external energy source matched to the size and location of the detector, e.g. X-ray transmission to measure the linear attenuation coefficient. However, for active imaging with an internal, uncollimated energy source that emits radiation (photons) in all directions, sectional imaging results in poor photon utilization, e.g. imaging the distribution of a radionuclide injected intravenously into the human body. Large-area detectors that increase the solid angle coverage are constructionally feasible, but full three-dimensional image reconstruction is required to take advantage of the improved detection efficiency.

The theoretical work of Vainshtein et al.[2] demonstrated the possibility of full, three-dimensional reconstruction, provided all the necessary data are available. The extension of two-dimensional techniques to three-dimensions is straightforward, although they make much heavier demands on computer time and storage than do their two-dimensional counterparts. Approaches based on iterative methods[3], the projection theorem[4], filtered back-projection[5], and Fourier deconvolution[6] have all been attempted, with variable success.

The situation is rather different if all the necessary data are not available. One example of an imaging system that generates an incomplete data set is a positron camera, consisting of two large-area, stationary detectors[7]. This camera measures in coincidence the positions of photon pairs arising from positron annihilation. Since the photons from a coincident pair are emitted 180° apart, the positional measurements define a line at some angle within the acceptance of the camera. The absence of data for angles outside the acceptance of the camera is equivalent to unmeasured projections at these angles. Any three-dimensional reconstruction algorithm for a large-area, stationary positron camera must therefore allow for the difficulties arising from the incomplete data set.

Several authors[8,9] have considered this problem of missing projections, and it has recently been suggested[10,11] that the data set may be completed by mathematical continuation methods, if the distribution to be reconstructed is of finite extent. These methods are known to be highly sensitive to measurement errors, but the iterative approach suggested by Papoulis[12] seems to offer some improvement.

This paper examines the problems associated with reconstruction for a positron camera with limited angular acceptance, based on the Fourier deconvolution method, without subsequent mathematical continuation. A closed-form expression for the appropriate deconvolution filter is given in Section 3, and examples of the reconstruction of both computer-simulated images and real data from a high resolution positron camera are provided in Sections 6 and 7, respectively.

2. Fourier Deconvolution for Positron Emission Imaging

Transmission-computed tomography is the technique whereby a two-dimensional section representing the distribution of attenuation coefficients is reconstructed from a sequence of one-dimensional projections. Each projection consists of a set of integrals of attenuation taken along different lines through the section, all lines being at the same angle for a given projection. Commencing with such a sequence of projections, a two-dimensional image may be formed by reprojecting the attenuation integrals back through the region of interest, assigning to each picture element (pixel) along the path a value proportional to the line integral. It is well known that this simple process, usually called back-projection, produces a distorted image of the true attenuation distribution. The distortion may be removed by filtering the one-dimensional projections before back-projection[13], or by filtering the two-dimensional distribution generated by the back-projection process[14]. The two approaches are mathematically equivalent, but the former is to be preferred from the viewpoint of implementation.

A similar situation arises in emission-computed tomography using positrons. The principles of positron emission tomography have been described by many authors[15], and they are summarized in Fig. 1 for the case of a large-area, stationary positron camera. The details of the camera, which is based on the high density, multiwire proportional chamber (MWPC), are discussed in a companion paper[16]. The reconstruction

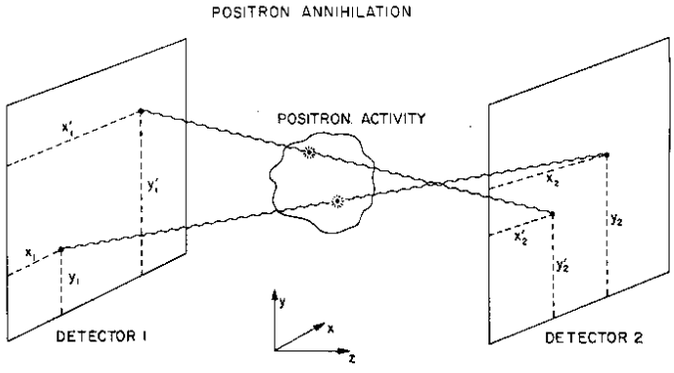

Fig. 1 Positron imaging with a large-area stationary camera

problem is to determine the positron activity distribution by measuring, in coincidence, many annihilation photon pairs, each pair giving a line through the activity distribution along which the annihilation occurred. The detectors may be considered as two-dimensional arrays of sensitive elements, and an element in one detector may be in coincidence with any element in the opposing detector. A pair of such elements defines a coincidence channel.

The annihilation pairs are emitted at all possible angles, and it is evident that to achieve a high sensitivity and a low radiation dose, the detector system should cover as large a solid angle as possible. Although the photon pairs are detected in an arbitrary order, pairs generating lines within the same coincidence channel may subsequently be summed to give an estimate, for a sufficiently large number of annihilations, of the isotope activity lying within that channel. However, photons emitted internally are subject to attenuation between their point of emission (a) and their point of detection (b) according to the usual exponential $\exp\left[-\int_a^b \mu(s)\,ds\right]$, where $\mu(s)$ is the attenuation coefficient along the channel s. For positron annihilation, both photons are attenuated and the product of the two exponential factors yields a depth-independent correction $\exp\left[-\int_0^L \mu(s)\,ds\right]$, where L is the total length of the channel. This correction factor may be obtained from a transmission study.

After correction for attenuation, the emission signal in a given coincidence channel is an estimate of the line integral of activity, just as in the transmission case the logarithm of the transmission signal is an estimate of the line integral of photon attenuation coefficients. A collection of all coincidence channels with the same polar angles represents a two-dimensional projection of the radionuclide activity. Two major differences with the normal transmission-computed tomography are apparent: i) the reconstruction should be fully three-dimensional if maximum use is to be made of available detection channels; and ii) projections are available for only a limited range of angles, compared with two-dimensional tomography where usually the full 2π angular range is covered.

The radionuclide distribution f(x,y,z) is to be reconstructed within a three-dimensional matrix of volume elements (voxels) as shown in Fig. 2. Given the two-dimensional projections, and by analogy with transmission-computed tomography, two approaches are open. Firstly, back-projection of the two-dimensional projections into the three-dimensional object space with subsequent three-dimensional filtering to remove the distortions; and secondly, two-dimensional filtering of the projections before back-projection into the object space. For this application, the first approach is preferred

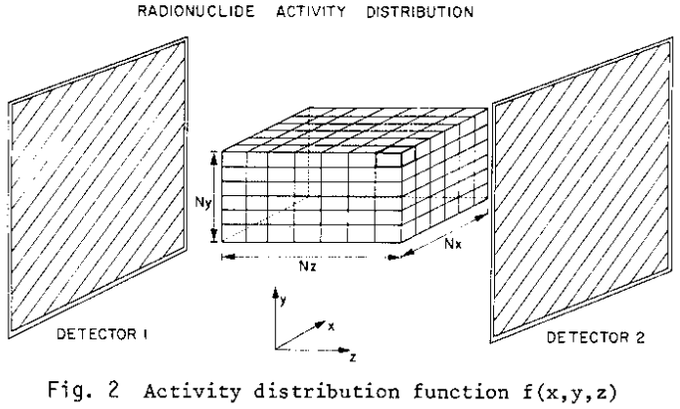

Fig. 2 Activity distribution function f(x,y,z)

for two reasons: i) the annihilation events are detected one at a time at random orientations, and back-projection may be performed immediately, event by event, avoiding data sorting or storage of the projections, and ii) the number of possible coincidence channels is large compared with the number of events detected in a reasonable time, and each projection is statistically poorly measured; since filtering is a noise amplification process, it is better to average the projection data by back-projection before filtering. A disadvantage is the necessity for three-dimensional Fourier transforms.

As in the two-dimensional case, the back-projected image $\hat{f}(x,y,z)$ is a distorted estimate of the real activity f(x,y,z). Since any general distribution may be regarded as a superposition of multiple point sources (impulses), it is sufficient to consider the distortion (blurring) of a single impulse by the back-projection process, weighted with the appropriate impulse amplitude and integrated over all possible point-source positions. Thus, if $h(x,y,z;\, x',y',z')$ is a function which represents a unit impulse at (x',y',z') after back-projection, a general back-projected distribution is related to the true activity distribution by

$$\hat{f}(x,y,z) = \int_{-\infty}^{\infty}\int\int\int f(x',y',z') \times \times h(x,y,z;\, x',y',z')\, dx'\, dy'\, dz' \,. \qquad (1)$$

Activity distributions of interest will be of finite extent since they represent, for example, the localization of a radionuclide within the human body. Thus, if $f(x',y',z')$ is confined within a region $0 \le x' \le X'$, $0 \le y' \le Y'$, $0 \le z' \le Z'$, Eq. (1) reduces to

$$\hat{f}(x,y,z) = \int_0^{X'}\int_0^{Y'}\int_0^{Z'} f(x',y',z') \times \times h(x,y,z;\, x',y',z')\, dx'\, dy'\, dz' \,. \qquad (2)$$

Equation (2) is a Fredholm integral equation of the first kind. Such equations usually express a very ill-conditioned problem, i.e. small fluctuations (noise) in $\hat{f}(x,y,z)$ generate much larger fluctuations in the solution $f(x',y',z')$. Equation (2) is avoided in its full generality if restrictions are placed on the coincidence channels used to generate $\hat{f}(x,y,z)$ such that the impulse transformation function $h(x,y,z;\; x',y',z')$ is space invariant, i.e. it depends only on the differences $x-x'$, $y-y'$, $z-z'$ and not on the actual values. The transformation then becomes a convolution:

$$\hat{f}(x,y,z) = \int_0^{X'}\int_0^{Y'}\int_0^{Z'} f(x,y,z) \times \times h(x-x',y-y',z-z')\, dx'\, dy'\, dz' \,. \qquad (3)$$

Two approaches have been proposed for solving this equation, both based on the Fourier convolution theorem[17], which transforms a convolution in real space into a point-wise product in Fourier space. One approach[18], using the convolution theorem in two dimensions (x,y), requires a matrix inversion at each spatial frequency (k_x,k_y) in order to solve the remaining one-dimensional convolution in z. The second

method[19], adopted here, is to use the Fourier transform of Eq. (3) in three dimensions, so that it reduces to

$$\hat{F}(k_x,k_y,k_z) = F(k_x,k_y,k_z)H(k_x,k_y,k_z) \ , \qquad (4)$$

where

$$\hat{F}(k_x,k_y,k_z) = \int_{-\infty}^{\infty}\iiint \hat{f}(x,y,z)\ e^{-2\pi i(xk_x+yk_y+zk_z)}\ dx\ dy\ dz \qquad (5a)$$

$$F(k_x,k_y,k_z) = \int_{-\infty}^{\infty}\iiint f(x,y,z)\ e^{-2\pi i(xk_x+yk_y+zk_z)}\ dx\ dy\ dz \qquad (5b)$$

$$H(k_x,k_y,k_z) = \int_{-\infty}^{\infty}\iiint h(x,y,z)\ e^{-2\pi i(xk_x+yk_y+zk_z)}\ dx\ dy\ dz \ . \qquad (5c)$$

In Section 3, a closed-form expression for $H(k_x,k_y,k_z)$ that results from explicitly evaluating Eq. (5c) will be given. It will be seen that for a limited-angle system, there is a cone of frequencies for which $H(k_x,k_y,k_z)$ is zero. The solution of Eq. (4) by simple division:

$$F_R(k_x,k_y,k_z) = \frac{\hat{F}(k_x,k_y,k_z)}{H(k_x,k_y,k_z)} \ , \qquad (6)$$

is permitted only if $H \neq 0$. Defining a generalized inverse[20] $G(k_x,k_y,k_z)$ by

$$G(k_x,k_y,k_z) = \begin{cases} H^{-1}(k_x,k_y,k_z) & \text{if} \quad H \neq 0 \\ 0 & \text{if} \quad H = 0 \end{cases} \qquad (7)$$

the solution of Eq. (4) becomes

$$F_R(k_x,k_y,k_z) = \hat{F}(k_x,k_y,k_z)G(k_x,k_y,k_z) \ . \qquad (8)$$

The reconstructed radionuclide distribution is then obtained from the inverse Fourier transform of Eq. (8):

$$f_R(x,y,z) = \int_{-\infty}^{\infty}\int_{-\infty}^{\infty}\int_{-\infty}^{\infty} F_R(k_x,k_y,k_z) \times \times\ e^{+2\pi i(xk_x+yk_y+zk_z)}\ dk_x\ dk_y\ dk_z \ . \qquad (9)$$

The case of missing frequencies also creates problems for the alternative approach of matrix deconvolution. At low spatial frequencies, a complex coupling of the measured and missing frequencies results in the matrices to be inverted being of low rank. Special inversion techniques, such as singular value decomposition[21], are required. The Fourier deconvolution approach is to be preferred since it allows a straightforward distinction between measured and unmeasured frequencies.

Any practical implementation of the above algorithm will involve sampled functions and the use of the fast Fourier transform (FFT). The back-projection distribution is expressed in a discrete three-dimensional grid (as shown in Fig. 2), and the solution $f_R(x,y,z)$ is calculated in this same grid. In fact, the corresponding discrete form of Eq. (2),

$$\hat{f}(i,j,k) = \sum_{i'}\sum_{j'}\sum_{k'} f(i',j',k')h(i',j',k';\ i,j,k) \ , \qquad (10)$$

may be solved directly without recourse to the convolution theorem, thereby eliminating the stringent space-invariance constraint. Such methods[22], although often more stable with respect to noise, are more demanding in computer time.

3. Derivation of the Filter, $G(k_x,k_y,k_z)$

A closed-form expression for the filter is obtained by evaluating the Fourier transform of the impulse function:

$$H(k_x,k_y,k_z) = \int_{-\infty}^{\infty}\iiint h(x,y,z)\ e^{-2\pi i(xk_x+yk_y+zk_z)}\ dx\ dy\ dz \ . \qquad (5c)$$

The three-dimensional integration can be performed numerically, but sufficient precision must be ensured in order to avoid spurious oscillations in the result. However, an analytic expression is to be preferred since it allows greater flexibility and simple evaluation at any frequency and to any precision. A closed-form expression for the case of a large-area rotating system has been evaluated by Colsher[6], using the appropriate circular symmetry of the impulse response function. In this section, the result for a stationary system will be given.

The back-projection of annihilation events from a single point-source of activity midway between the detectors yields a conical distribution of semiangle ψ and square cross-section (for square detectors). Space invariance demands that this distribution appears the same for all points within the reconstruction region, so that the angle ψ is smaller than the maximum allowed by the detector aperture (see Fig. 3). Within the cone, the function varies as the inverse square of the distance from the point source, with an additional factor of cos θ if the annihilation lines are intersected with planes parallel to the detectors instead of with three-dimensional voxels (θ in the angle between the annihilation line and the z-axis). The appropriate impulse response function is therefore[22]

$$h(x,y,z) = \frac{\cos\theta}{2\pi r^2} = \frac{z}{2\pi(x^2+y^2+z^2)^{3/2}} \ . \qquad (11)$$

Substituting Eq. (11) into Eq. (5c) and inserting the appropriate limits for the acceptance angle, the integral to be evaluated is:

$$H(k_x,k_y,k_z) = \frac{1}{2\pi}\int_0^{\infty}\int_{-z\tan\psi}^{+z\tan\psi}\int_{-z\tan\psi}^{+z\tan\psi} \frac{z}{(x^2+y^2+z^2)^{3/2}} \times \times\ e^{-2\pi i(xk_x+yk_y+zk_z)}\ dx\ dy\ dz \ . \qquad (12)$$

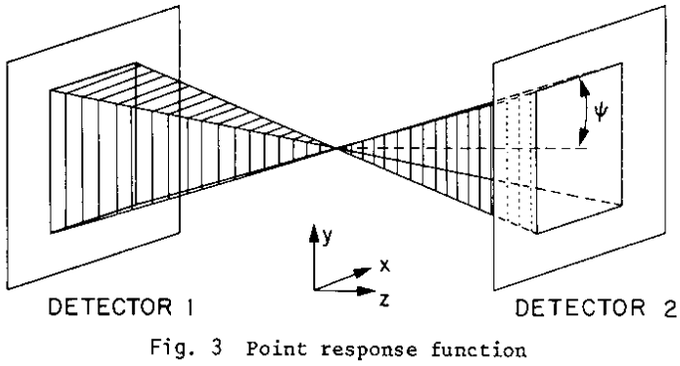

Fig. 3 Point response function

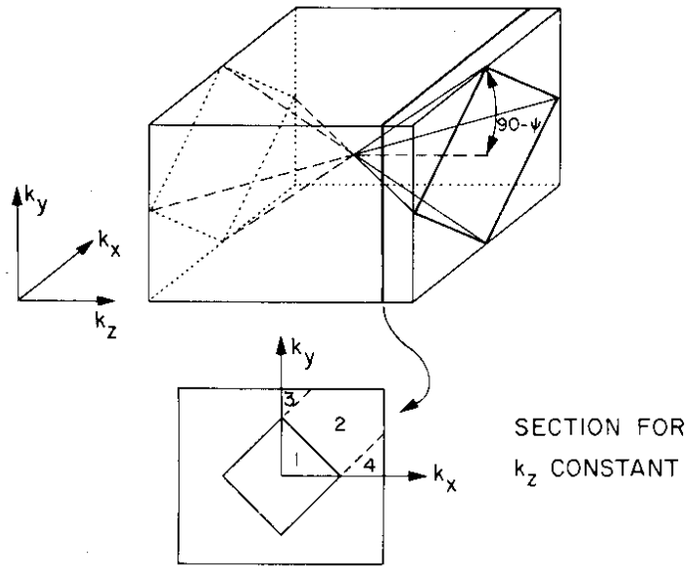

Fig. 4 The function $H(k_x,k_y,k_z)$

The evaluation is rather lengthy and the details will be reported elsewhere[23]. The result is a frequency space function for which four different regions can be identified, as shown in Fig. 4. The value of the function in each region is given by:

Region 1: $k_z > (k_x + k_y) \tan\psi$

$$H(k_x,k_y,k_z) = 0 \ . \qquad (13a)$$

Region 2: $\tan\psi\,|k_x - k_y| \le k_z \le \tan\psi\,(k_x + k_y)$

$$H(k_x,k_y,k_z) = \frac{1}{2k^2}(q_1 + q_3) \ . \qquad (13b)$$

Region 3: $k_y \ge k_x;\ 0 \le k_z \le \tan\psi\,(k_y - k_x)$

$$H(k_x,k_y,k_z) = \frac{1}{2k^2}(q_3 + q_4) \ . \qquad (13c)$$

Region 4: $k_x \ge k_y;\ 0 \le k_z \le \tan\psi\,(k_x - k_y)$

$$H(k_x,k_y,k_z) = \frac{1}{2k^2}(q_1 + q_2) \ , \qquad (13d)$$

where

$$q_1 = \frac{\tan\psi\,(k_x^2 + k_y^2) - k_y k_z}{\left[(1 + \tan^2\psi)k_x^2 + (k_z - k_y\tan\psi)^2\right]^{1/2}}$$

$$q_2 = \frac{\tan\psi\,(k_x^2 + k_y^2) + k_y k_z}{\left[(1 + \tan^2\psi)k_x^2 + (k_z + k_y\tan\psi)^2\right]^{1/2}}$$

$$q_3 = \frac{\tan\psi\,(k_x^2 + k_y^2) - k_x k_z}{\left[(1 + \tan^2\psi)k_y^2 + (k_z - k_x\tan\psi)^2\right]^{1/2}}$$

$$q_4 = \frac{\tan\psi\,(k_x^2 + k_y^2) + k_x k_z}{\left[(1 + \tan^2\psi)k_y^2 + (k_z + k_x\tan\psi)^2\right]^{1/2}} \ .$$

These expressions are valid for $k_x \ge 0$, $k_y \ge 0$, $k_z \ge 0$; other values are obtained by symmetry. The vanishing of the function in region 1 is the consequence of the limited angular acceptance of the camera which implies the absence of projections at certain angles. From the projection theorem[5], a two-dimensional projection corresponds, in Fourier space, to a plane of frequencies at the same angle as the projection. The missing projections become planes of unmeasured frequencies, which, for the square acceptance cone (Fig. 3) results in a square, but rotated, cone of missing frequencies in Fourier space (Fig. 4).

For a system without angular limitations, the three-dimensional Fourier transform of the impulse response function $1/2\pi r^2$ may be calculated[24], using the theory of generalized functions[25], to give the result

$$H(k_x,k_y,k_z) = \frac{1}{2k} \ , \qquad (14)$$

where k is the spatial frequency radius in three dimensions. The filter, $H^{-1}(k_x,k_y,k_z) = 2k$, is thus the familiar ramp function encountered in two-dimensional reconstruction from projections. To investigate the limiting behaviour of the filter given in Eq. (13), a conversion to polar coordinates shows that all the functions are of the form:

$$H(k,\Theta,\Phi) = \frac{1}{2k} D_R(\Theta,\Phi;\ \tan\psi) \ , \qquad (15)$$

where the angular part, $D_R(\Theta,\Phi;\ \tan\psi)$ depends upon the particular region R. For example, in the $k_z = 0$ plane, Eq. (15) becomes

$$H(k,\Phi) = \frac{1}{4k}\left(1 + \frac{\cos^2\Phi}{\tan^2\psi}\right)^{-1/2} \ , \quad 0 \le \Phi \le \frac{\pi}{4} \ . \qquad (16)$$

In the limit of full angular acceptance, as $\psi \to \pi/2$, Eq. (16) reduces to Eq. (14) with an extra factor of 2 coming from the cos θ in Eq. (12).

4. High-Frequency Noise

It is well known that the filtering operation represented by Eq. (8) is extremely sensitive to noise in the function $\hat{F}$[26]. This comes from the basic ill-conditioning of the Fredholm integral equation [Eq. (2)], and from the fact that any practical implementation of Eq. (8) is for a finite range of frequencies. For a sampled function such as $\hat{F}$, a natural choice for the high-frequency limit that avoids aliasing[17] problems is the Nyquist frequency. However, the filter [Eq. (13)] increases with increasing frequency, while the camera response in general decreases with increasing frequency. The higher frequencies below the Nyquist limit are often seriously affected by noise coming from statistical fluctuations in $\hat{f}(x,y,z)$. To avoid over-emphasizing the effects of this noise during filtering, it is important to tailor the filter to the frequency response of the camera. In addition, a sharp cut-off in the filter at the Nyquist frequency can cause spurious oscillations that introduce artifacts into the reconstruction.

Functions which perform this tailoring operation on the filter are called window functions. The function to be used in Eq. (8) in place of G is therefore

$$G_W(k_x,k_y,k_z) = G(k_x,k_y,k_z)W(k_x,k_y,k_z) \ ,$$

where $W(k_x,k_y,k_z)$ is the window function. There are many possible choices for $W(k_x,k_y,k_z)$ [27]; the reconstructions presented in the next sections have been obtained using a Hanning window:

$$W(k) = \frac{1}{2}\left[1 + \cos\left(\pi k/k_c\right)\right] \ , \qquad k \le k_c \ ,$$

$$= 0 \text{ otherwise} \ .$$

An alternative choice, proposed by Chu and Tam[19], was obtained from an extension of Phillip's smoothness criterion[26] to three-dimensions. The result was a window of the form

$$W(k_x,k_y,k_z) = \frac{1}{1 + \gamma k^4 G^2} ,$$

which has a dependence on the filter itself. The constant γ (Lagrange multiplier) is chosen according to the noise level in $\hat{f}(x,y,z)$; $\gamma = 0$ would correspond to a sharp truncation of the filter.

5. Summary of the Algorithm

The filtering process is summarized in Fig. 5, for a point source of activity at the mid-position between the two detectors. The distribution of activity on a horizontal plane through the centre of the source is shown on the right. In (a) the original activity appears as a peak, with a finite width originating from a combination of source size and detector resolution.

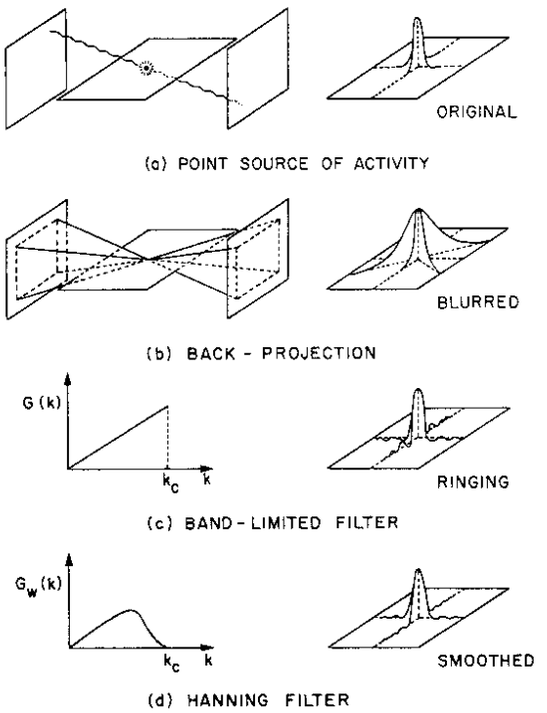

Fig. 5 The filtering process

In (b) the familiar cone-shaped distribution resulting from back-projection is shown, with the blurring (proportional to $1/r^2$) in the direction perpendicular to the detectors. As a result of the filtering [Eq. (8)] with a function indicated schematically in one dimension as a ramp function with sharp truncation, the blurring due to back-projection is removed, but oscillations (caused by the sharp truncation) are introduced (Fig. 5c). The oscillations are reduced (Fig. 5d) at the expense of a slight increase in the width of the reconstructed peak, by a smoother approach of the filter to the Nyquist cut-off (k_c): in practice, the full filter is three-dimensional [Eq. (13)].

6. Application to Simulated Data

The reconstruction process described above has been tested on computer-simulated images. Detailed results will be published elsewhere[28], but two examples, a point source and a tumour simulation, are presented here.

6.1 Point Source

A simulated point source consisting of a single element of activity at the mid-point of the camera was back-projected and filtered using Eqs. (8) and (13), and a section through the centre of the source is shown in Fig. 6 for both the x and the z direction in the xz plane. The filter is effective in removing the distortion due to back-projection in the z direction, but a sharp truncation causes an undershoot of about 16% in the x direction. This is somewhat reduced by a Hanning window.

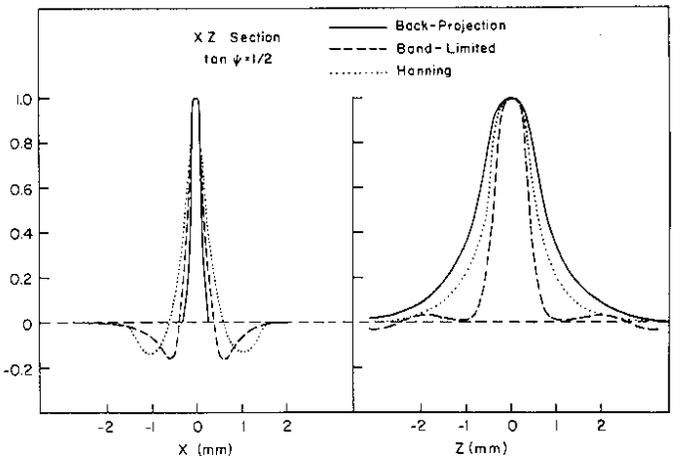

Fig. 6 Simulated point source

6.2 Tumour Simulation

The result of reconstructing a simulation consisting of a cylindrical "skull" surrounding two hemispherical "brain" distributions, one of which contains a hot spot representing a tumour, is displayed in Fig. 7. Four tomographic sections are shown corresponding to different levels through the skull. The

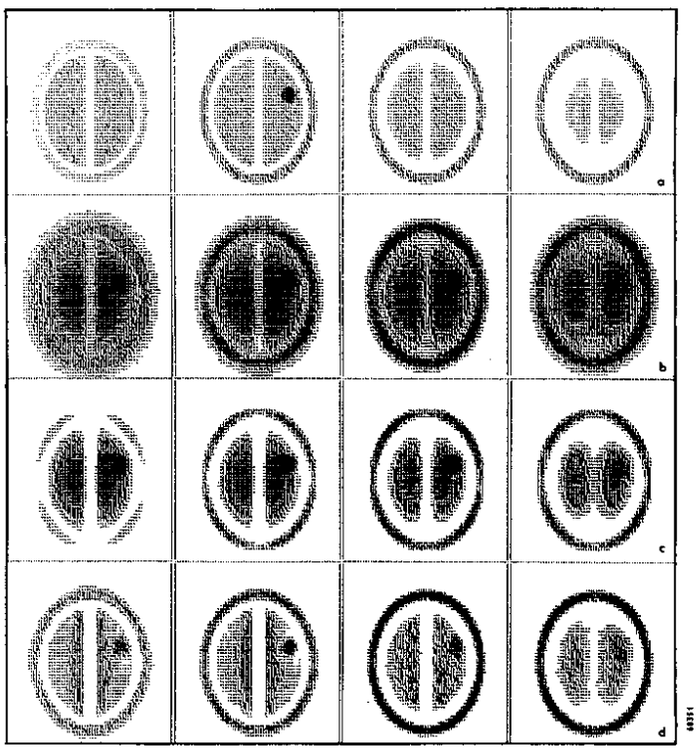

Fig. 7 Tumour simulation -- tomographic sections

pixel size is 1 mm × 1 mm and the distance between sections is 10 mm. The original simulation is shown in Fig. 7a, and the distorted, back-projected image in Fig. 7b, where shadowing of the tumour onto adjacent planes is apparent. Subjecting the back-projected image to a 50% linear background subtraction (Fig. 7c) slightly improves the contrast, but agreement with the original is poor because the background is non-linear. Reconstruction with a Hanning window is shown in Fig. 7d; back-projection distortion is reduced and agreement with the original is much better.

7. Application to Real Data

In this section, some examples of the reconstruction of real images from a high-resolution positron camera are presented. The details of the camera and further examples of images can be found in a companion paper[16] and elsewhere[29].

7.1 Point Source

Approximately 100000 events were collected from a 1 mm diameter point source of ^{22}Na positioned at the mid-point of the camera. After back-projection and filtering, sections through the centre of the source in the x and z direction for the xz plane appear as in Fig. 8. For such a high contrast, high statistics image, the best results were obtained with a rather sharp cut-off in the z-direction and a smoother truncation in the x-direction.

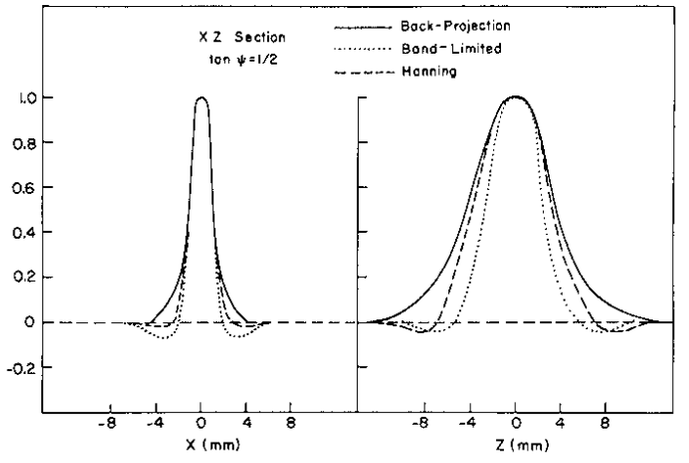

Fig. 8 ^{22}Na point source

7.2 An Isolated Heart

In practice, images will contain far fewer events per volume element than the previous point-source situation, and statistical noise will limit the spatial resolution ultimately obtainable. In addition, the rather high level (40%-50%) of accidental, random coincidences accepted by the camera will serve to further increase the statistical noise without contributing to the signal.

The chambers of an isolated, human heart were filled with a solution of ^{68}Ga of total activity 300 μCi. The heart was placed between the detectors and approximately three million events were collected. Figure 9 shows a single cross-section containing about 100,000 signal events with a pixel size of 2 mm × 2 mm. The measured[29] spatial resolution of the camera for ^{68}Ga has a full width at half maximum of 3.5 mm, with a high-frequency cut-off in the corresponding modulation transfer function of about 2.5 cm^{-1}. The reconstructions of Fig. 9 are for a) sharp cut-off, k_c = 2.5 cm^{-1}; b) Hanning, k_c = 2.5 cm^{-1}; c) Hanning, k_c = 1.65 cm^{-1};

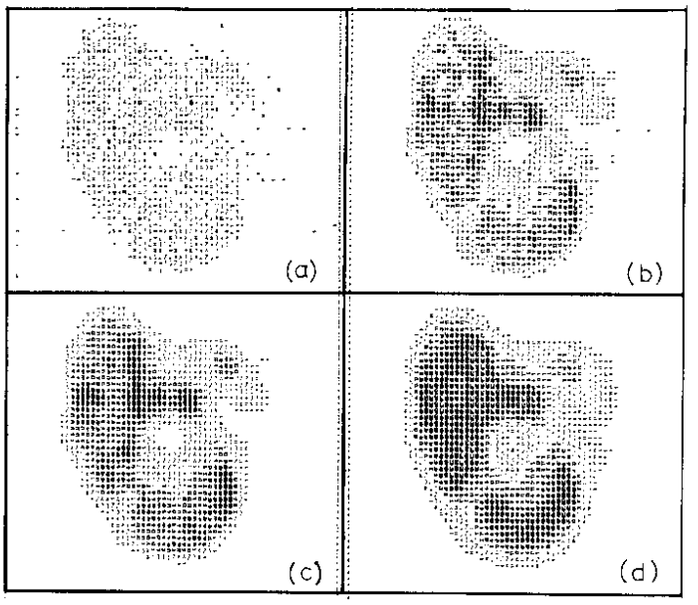

Fig. 9 Cross-section of a human heart

and d) Hanning, k_c = 1.125 cm^{-1}. The increased smoothing is apparent as the filter cut-off frequency (k_c) is lowered, and the statistical limitations and spurious oscillations of a sharp cut-off are clearly seen in Fig. 9a. A smoother approach to the cut-off frequency (Fig. 9b) reduces fluctuations, but false detail is still visible.

7.3 *In vivo* Imaging

A live rabbit was injected intraveneously with 130 μCi of a bone-labelling tracer[30] ^{68}Ga-DTPMP. After 1½ hours the animal was anaethetized and an image taken with the longitudinal axis in a plane parallel to the detector plane. In Fig. 10 a single tomographic section

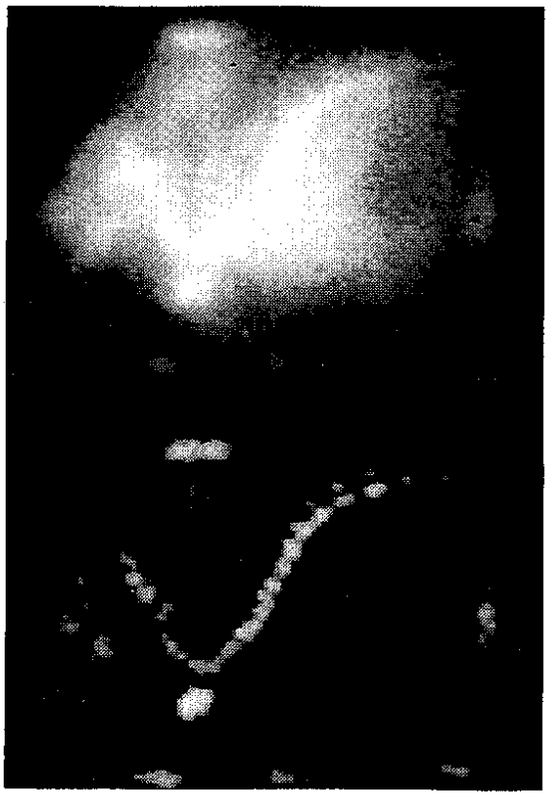

Fig. 10 Tomographic section of a rabbit

is shown for a) the back-projected image and b) the image after filtering. Only the front portion of the rabbit was within the camera field of view, but the spine, skull, lower jaw bone, front legs, and even individual vertibrae are clearly seen on the filtered image. Such detail is obscured by distortions in the back-projected image.

8. Conclusion

This paper has considered the problems of three-dimensional image reconstruction for a limited-angle, positron camera using the approach of Fourier deconvolution. The difficulties specific to a limited-angle stationary system have been examined, and an analytic expression of the filter appropriate for a system with a conical impulse response function has been given.

The filter has been tested extensively on both real and simulated data, and examples demonstrating the effectiveness of the method are provided.

Acknowledgements

The authors are indebted to K. Kull, C. Rivoiron, G. Roubaud, B. Lindberg and G. Lee from CERN, and P. Frey and A. Donath from the Department of Nuclear Medicine, Cantonal Hospital, Geneva, for help with the construction and operation of the camera and in producing the images shown in Section 6. The bone-labelling agent ^{68}Ga-DTPMP was provided by G. Banna, whose assistance is gratefully acknowledged. The authors thank E. Gabathuler, Experimental Physics Division, CERN, for his support and encouragement.

REFERENCES

1. J. Radon, On the determination of functions from their integrals along certain manifolds, Ber. Saechs. Akad. Wiss. (Leipzig) Math.-Phys. Kl 69, 262 (1917).

2. B.K. Vainshtein and S.S. Orlov, *in* Techniques of three-dimensional reconstruction, Proc. Int. Workshop, Brookhaven National Laboratory, Upton, New York, 16-19 July (1974).

3. J.G. Colsher, Iterative three-dimensional image reconstruction from tomographic projections, Computer Graphics and Image Processing 6, 513 (1977).

4. R.A. Crowther, D.J. DeRosier and A. Klug, The reconstruction of a three-dimensional structure from projections and its applications to electron microscopy, Proc. Roy. Soc. (London) Ser. A 317, 319 (1970).

5) N.J. Pelc and D.A. Chesler, Utilization of cross-plane rays for three-dimensional reconstruction by filtered back-projection, J. Comput. Assist. Tomogr. 3 (3), 385 (1979).

6. J.G. Colsher, Fully three-dimensional positron emission tomography, Submitted to Phys. Med. Biol. (1979).

7. A.P. Jeavons, D.W. Townsend, N.L. Ford, K. Kull, A. Manuel, O. Fischer and M. Peter, A high resolution proportional chamber positron camera and its applications, IEEE Trans. Nucl. Sci. NS-25, 1, 164 (1978).

8. B. Macdonald, C.B. Lim, V. Perez-Mendez and K.C. Tam, A comparison of three three-dimensional reconstruction methods for large-area positron cameras, J. Comput. Assist. Tomogr. 2 (5), 642 (1978).

9. H. Tuy, Reconstruction of a three-dimensional object: Limited range of views, S.U.N.Y. (at Buffalo), MIPG 17 (1979).

10. H. Tuy, Radon transform in the space of distributions of compact support, S.U.N.Y. (at Buffalo), MIPG 21 (1979).

11. K.C. Tam, V. Perez-Mendez and B. Macdonald, Reconstruction in emission and transmission tomography with limited-angle input, IEEE NS-26 (2), 2797 (1979).

12. A. Papoulis, IEEE Trans. Circuits and Syst., CAS-22, 735 (1975).

13. T.F. Budinger and G.T. Gullberg, Three-dimensional reconstruction in nuclear medicine emission imaging, IEEE Trans. Nucl. Sci. NS-21, 2 (1974).

14. P.R. Smith, T.M. Peters and R.H.T. Bates, Image reconstruction from a finite number of projections, J. Phys. A 6, 361 (1973).

15. M.E. Phelps, Seminars in Nuclear Medicine 7, 337 (1977).

16. A. Jeavons, K. Kull, B. Lindberg, G. Lee, D. Townsend, P. Frey and A. Donath, A proportional chamber positron camera for medical imaging, Presented at this Conference.

17. E.O. Brigham, The fast Fourier transform (Prentice-Hall, Englewood Cliffs, N.J., 1974), p. 58.

18. L.T. Chang, B. Macdonald and V. Perez-Mendez, Axial tomography and three-dimensional image reconstruction, LBL-3872 (1975).

19. G. Chu and K.C. Tam, Three-dimensional imaging in the positron camera using Fourier techniques, Phys. Med. Biol. 22, 245 (1977).

20. R. Prost and R. Goutte, Deconvolution when the convolution kernal has no inverse, IEEE Trans. Acoust., Speech and Signal Process ASSP-25, 6, 542 (1977).

21. D. Townsend, C. Piney and A. Jeavons, Object reconstruction from focused positron tomograms, Phys. Med. Biol. 23, 235 (1978).

22. F.B. Atkins, G. Muehllehner and P.V. Harper, Proc. 5th Int. Conf. on Information Processing in Medical Imaging, Nashville, Tenn., 1977, p. 195.

23. B. Schorr and D. Townsend, Analytic evaluation of a filter for positron image reconstruction, To be submitted to Phys. Med. Biol. (1979).

24. E. Tanaka, Generalized correction functions for convolutional techniques in three-dimensional image reconstruction, Phys. Med. Biol. 24, 157 (1979).

25. M.J. Lighthill, Fourier analysis and generalized functions, Cambridge University Press (1958).

26. D.L. Phillips, A technique for the numerical solution of certain integral equations of the first kind, J. Assoc. Comput. Mach. 9, 84 (1962).

27. S.W. Rowland, Computer implementation of image reconstruction formulas, S.U.N.Y. (at Buffalo), MIPG Technical Report No. 3 (1978).

28. D. Townsend, B.-M. Bleichert and B. Schorr, A quantitative comparison of various filters for positron image reconstruction, To be submitted to Phys. Med. Biol.

29. A. Jeavons, The CERN proportional chamber positron camera, CERN-EP/79-59 (1979).

30. M.K. Dewanjee, D.J. Hnatowich and R. Beh, New ^{68}Ga-labelled skeletal imaging agents for positron scintigraphy, J. Nucl. Med. 17, 1003 (1976).